

Accepted Manuscript

Pyrolytic synthesis of MoO_3 nanoplates within foam-like carbon nanoflakes for enhanced lithium ion storage

Daxian Cao, Yanzhu Dai, Sanmu Xie, Hongkang Wang, Chunming Niu

PII: S0021-9797(17)31467-4
DOI: <https://doi.org/10.1016/j.jcis.2017.12.077>
Reference: YJCIS 23149

To appear in: *Journal of Colloid and Interface Science*

Received Date: 19 November 2017
Revised Date: 24 December 2017
Accepted Date: 27 December 2017

Please cite this article as: D. Cao, Y. Dai, S. Xie, H. Wang, C. Niu, Pyrolytic synthesis of MoO_3 nanoplates within foam-like carbon nanoflakes for enhanced lithium ion storage, *Journal of Colloid and Interface Science* (2017), doi: <https://doi.org/10.1016/j.jcis.2017.12.077>

This is a PDF file of an unedited manuscript that has been accepted for publication. As a service to our customers we are providing this early version of the manuscript. The manuscript will undergo copyediting, typesetting, and review of the resulting proof before it is published in its final form. Please note that during the production process errors may be discovered which could affect the content, and all legal disclaimers that apply to the journal pertain.



Pyrolytic Synthesis of MoO₃ Nanoplates within Foam-like Carbon Nanoflakes for Enhanced Lithium Ion Storage

Daxian Cao,^a Yanzhu Dai,^a Sanmu Xie,^a Hongkang Wang,^{a*} and Chunming Niu^a

^a Center of Nanomaterials for Renewable Energy (CNRE), State Key Lab of Electrical Insulation and Power Equipment, School of Electrical Engineering, Xi'an Jiaotong University, Xi'an, China 710049. E-mail: hongkang.wang@mail.xjtu.edu.cn (H. Wang)

^bState Key Laboratory for Mechanical Behavior of Materials & School of Microelectronics, Xi'an Jiaotong University, Xi'an 710049, China.

Abstract

MoO₃ as electrode material for lithium ion batteries (LIBs) suffers from the poor ionic and electronic conductivity, while hybridizing nanostructured MoO₃ with carbon-based materials is regarded as an efficient strategy. Herein, we report the facile synthesis of MoO₃ nanoplates within foam-like carbon nanoflakes (CNFs) via the pyrolysis of molybdenum 2-ethylhexanoate (C₄₈H₉₀MoO₁₂) at a low temperature of 300 °C under ambient atmosphere. Mixing C₄₈H₉₀MoO₁₂ with the highly porous foam-like CNFs allows the sufficient pyrolysis of Mo precursor, which can readily crystallize into MoO₃ with plate morphology. The loading amount of MoO₃ within CNFs can be easily and precisely controlled by adjusting the relative amount of C₄₈H₉₀MoO₁₂ / CNFs, while the plate morphology of MoO₃ can be well preserved. The structural characteristics as well as the formation mechanism are investigated. When used as anode material for LIBs, optimized MoO₃/CNFs displays superior lithium storage performance, delivering a high discharge capacity of 791 mA h/g after 100 cycles at 500 mA/g and even ~600 mA h/g at a high rate of 2000 mA/g. Moreover, the present pyrolysis synthetic strategy can be generally applied for low-cost and large-scale fabrication of various MoO₃/carbon nanocomposites, which demonstrates

great potential in the development of high-performance electrodes for electrochemical energy-storage.

Keywords: *molybdenum 2-ethylhexanoate; MoO₃ nanoplates; pyrolysis synthesis; carbon nanoflakes; lithium storage*

Introduction.

Rechargeable lithium ion batteries (LIBs) have been widely used as power sources in the portable electronics and have great potentials in large-scale applications such as electric vehicles and smart-grid energy storage in future, owing to their high energy density, high working voltage and long lifespan as compared with other alternatives.[1-3] To date, the graphite anode in commercial LIBs cannot meet the increasing demand for higher energy density because of its lower theoretical capacity (372 mA h/g for graphite).[4] Molybdenum trioxide (MoO₃), with a higher theoretical capacity of 1117 mA h/g, has been regarded as a promising candidate anode material for LIBs because of its attractive characteristics, such as low cost, high thermal and chemical stability and environment benignity.[5] The lithium storage mechanism of MoO₃ is based on the reversible conversion reaction of $\text{MoO}_3 + 6\text{Li}^+ + 6\text{e}^- \leftrightarrow 3\text{Li}_2\text{O} + \text{Mo}$. [6-8] However, it is often limited by the poor ionic and electronic conductivity for the bulk MoO₃, finally resulting in the poor electrochemical performance. Besides, the volume changes and thus resultant pulverization problem of the active materials upon cycling is another key obstacle for achieving high-performance lithium storage.

Nanostructuring and carbon hybridization have been suggested as two efficient strategies to overcome the above-mentioned drawbacks. First, nanomaterials with large surface-to-volume ratio and small size exhibit novel structure-dependent physicochemical properties,[9] which can shorten the diffusion pathway of lithium ions and effectively release the strain produced by repeated lithation/delithiation upon cycling. Therefore, various nanostructured MoO₃ with different morphologies such as nanoparticles[10], nanowires[11], nanobelts[12, 13], nanorods[14, 15], and yolk-shell spheres[16], have been fabricated and showed enhanced electrochemical properties.

However, the performance improvement by nanostructuring was still quite limited, as the drastic structure destruction caused by large volume expansion upon lithiation usually happened after a short-term cycling. Furthermore, hybridizing MoO_3 with carbon-based materials has been one of the most effective solutions to address the above problem. Carbon materials especially with crystalline structure (ex., graphite, carbon nanotubes and graphene) possess prominent mechanical flexibility and electrical conductivity, which can not only accommodate the volume changes but also preserve the electrical contact during lithiation/delithiation upon cycling.

Thus, combined engineering on the MoO_3 nanostructures as well as their carbon hybridization in desired manners is of vital importance to improve the electrochemical performance. So far, many efforts have been devoted to the fabrication of orthorhombic $\alpha\text{-MoO}_3$ with peculiar layered structure, which offers rich intercalation chemistry and is more promising as LIB anode.[17, 18] Various strategies, such as hydrothermal method,[19, 20] chemical vapor deposition (CVD),[21] wet chemistry method,[22] have been used to fabricate crystalline MoO_3 nanofibers[23], nanobelts[19] and nanoplates structure[24]. However, these preparation routes are generally complicated and expensive; especially the CVD and hydrothermal method are not suitable for large-scale preparation. Alternately, solid-state synthesis by simply mixing the reactants and then annealing under certain atmosphere is easy to handle and can be scaled up. For example, Wang et al prepared MoO_3 nanoplate film on Si substrate by annealing the molybdenum isopropoxide ($\text{Mo}(\text{OC}_3\text{H}_7)_5$) and the poly(ethylene oxide) hybrid composite at 500°C in air.[22] However, the feasibility for large-scale powder production was not addressed and the reaction temperature was too high for the simultaneous carbon hybridization. In our previous reports, we realized the facile deposition of ultrafine SnO_2 nanoparticles on various carbon nanomaterials such as graphene, carbon nanotubes/nanoflakes via annealing the tin(II) 2-ethylhexanoate and carbon mixtures at a low temperature of 300°C in air, which showed superior electrochemical performance.[25, 26]

As is well known that MoO_3 crystallizes into three polymorphs, namely, orthorhombic $\alpha\text{-MoO}_3$, monoclinic $\beta\text{-MoO}_3$ and hexagonal h-MoO_3 , among which

α -MoO₃ has a layered structure with adjacent double-layers of MoO₆ octahedra linked by sharing edge and corner along the (001) and (100) axes by weak van der Waals forces along the (010) direction.[15] Owing to this peculiar layered structure, α -MoO₃ offers rich intercalation chemistry and is more promising as LIB anode. Herein, we reported a simple method to realize the shape-controlled growth of crystalline α -MoO₃ nanosheets within foam-like carbon nanoflakes (CNFs) (denoted as MoO₃/CNFs), by simply annealing the mixture of molybdenum 2-ethylhexanoate and CNFs in air at 300 °C, without the use of any surfactants. When used as anode materials, the as-prepared MoO₃/CNFs demonstrated superior lithium storage performance.

Experimental Section.

Materials synthesis. Foam-like carbon nanoflakes (CNFs) were prepared by a modified chemical vapor deposition method following our previous report.[27] In a typical synthesis, 3 g of the basic magnesium carbonate was placed into silica tube in a horizontal furnace, and temperature was ramped up to 1100 °C at a rate of 10 °C/min and kept for 30 min under Ar/CH₄ flow (90 sccm Ar and 10 sccm CH₄). After naturally cooling down to room temperature, CNFs were obtained by stirring the MgO@C product in excess aqueous HCl solution and washing thoroughly with distilled water until to the neutral pH value, which were then dried at 60 °C overnight for further use. In the typical synthesis of MoO₃/CNFs, 356 mg of molybdenum 2-ethylhexanoate and 20 mg of CNFs were both dispersed in ethanol under ultrasonic irradiation for 1 h, which was then transferred into an electric oven at 80 °C in order to completely evaporate the ethanol. The solid mixture was then annealed in air at 300 °C for 6 h, and the MoO₃/CNFs were finally obtained. The relative content of MoO₃ and CNFs can be readily controlled through changing the introduction amounts of molybdenum 2-ethylhexanoate and CNFs. In contrast, MoO_x sample was also prepared by solely annealing the molybdenum 2-ethylhexanoate in air at 300 °C for 6 h.

Materials Characterization. Powder X-ray diffraction (XRD) was applied to

characterize the phase structures of the product on a Bruker D2 PHASER X-ray diffractometer using Cu K α radiation ($\lambda=1.5418$ Å) with voltage at 30 kV and current at 10 mA. The morphologies of the products were characterized using a scanning electron microscope (SEM, FEI Quanta 250F) and transmission electron microscope (TEM) on a JEOL-2100 TEM operated at 200 kV. Raman spectroscopy was carried out using a Renishaw Raman RE01 scope with Ar excitation laser at 514 nm. Thermogravimetric analysis (TGA) was conducted in air with a heating rate of 5° C/min on a METTLER TOLEDO TGA/DSC thermal analyzer. The surface area and pore structures were examined using a Quantachrome Autosorb IQ analyzer.

Electrochemical Measurements. Electrochemical measurements were performed using CR2025 coin-type cells which were assembled in an Ar-filled glove box with both H₂O and O₂ contents less than 1.0 ppm. The working electrode was prepared by casting an aqueous slurry containing active material, acetylene black and poly acrylic acid binder with a weight ratio of 80:10:10, followed by drying at 120 °C under vacuum overnight. Lithium foil was used as the counter electrode, and Celgard 2400 microporous membrane was used as a separator. The electrolyte was prepared by dissolving 1 M LiPF₆ in a mixture of ethylene carbonate/dimethyl carbonate with volume ratio of 1:1. Galvanostatic discharge/charge tests were performed at various current densities in the voltage range of 0.01-3.0 V (vs. Li/Li⁺) on a LAND battery test system (Neware Technology Co., Ltd., China) at room temperature (25°C). Cyclic voltammetry (CV) was carried out on an electrochemical station (Autolab PGSTAT 302N) in the range of 0.01-3.0 V at a scan rate of 0.2 mV/s. Electrochemical impedance spectroscopy (EIS) was carried out with a voltage amplitude of 10 mV in the frequency range of 10 MHz to 0.01 Hz.

Results and discussion

Molybdenum 2-ethylhexanoate (C₄₈H₉₀MoO₁₂) is a viscous liquid, which can decompose upon high temperature treatment. After annealing in air at 300 °C, liquid C₄₈H₉₀MoO₁₂ converts into solid MoO_x product, which is amorphous with poor crystallinity as revealed by the XRD analysis (Figure 1a). Figure 1 b and c show the

SEM images of MoO_x product, which contains irregular particles with size up to tens of micrometers, and close observation reveals the presence of regular plates on the top surface (Figure 1c). This can be explained by the fact that the viscous liquid gradually condenses and becomes compact solid, while only the surface part exposed in air has the mobility for delicate recrystallization. To facilitate the dispersion of $\text{C}_{48}\text{H}_{90}\text{MoO}_{12}$ in a large surface area, foam-like carbon nanoflakes (CNFs) with large pore volume and high specific surface area were prepared by a modified chemical vapor deposition method following our previous work,[27] and Figure 1d shows the SEM image of the CNFs. Notably, when annealing the mixture of $\text{C}_{48}\text{H}_{90}\text{MoO}_{12}$ /CNFs, highly crystalline MoO_3 was obtained. As shown in the XRD pattern (Figure 1a), all diffraction peaks in MoO_3 /CNFs can be indexed to crystalline orthorhombic phase of MoO_3 (JCPDS No. 05-0508).

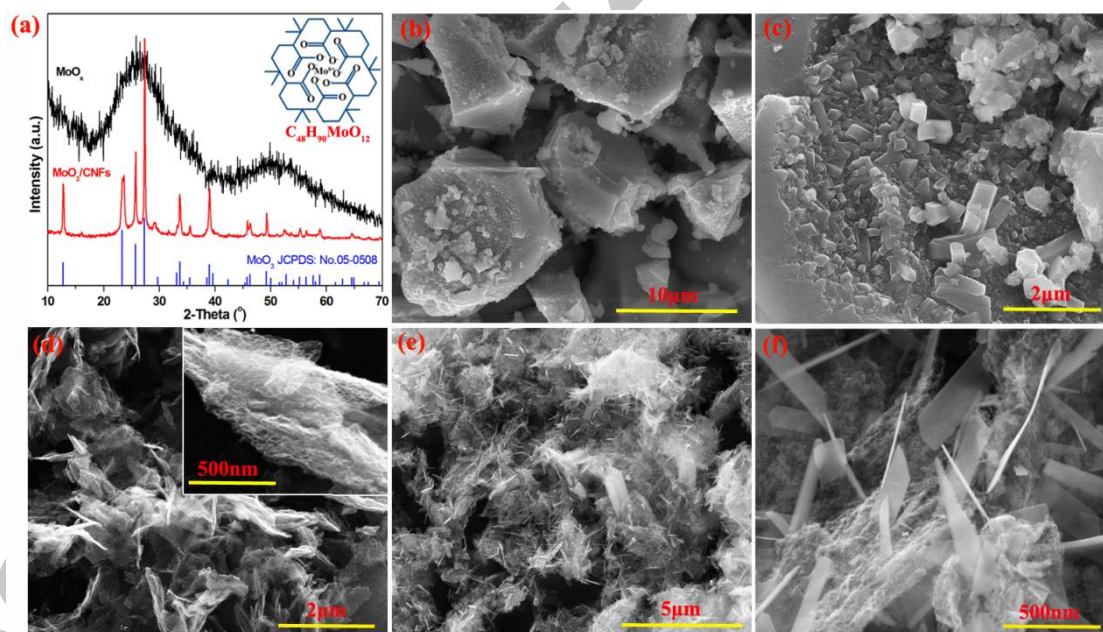


Figure 1. (a) XRD patterns of MoO_x and MoO_3/CNFs with inset showing the formula and molecule structure of the molybdenum 2-ethylhexanoate ($\text{C}_{48}\text{H}_{90}\text{MoO}_{12}$). (b-f) SEM images of the MoO_x (b, c), CNFs (d) and MoO_3/CNFs (e, f).

Figure 1e and f show the SEM images of the MoO_3/CNFs , in which MoO_3 interestingly exhibits a plate-like morphology, and the MoO_3 nanoplates are randomly interconnected with CNFs. Figure 2a shows the TEM image of the MoO_3/CNFs ,

where many MoO_3 nanoplates are attached but not grown on the foam-like CNFs. Figure 2b and c depict the cross-view and top-view lattice structures of single MoO_3 nanoplates, respectively, and the lattice spacing of 0.68 nm can be indexed to the (020) plane of MoO_3 (Figure 2b), while the lattice spacing of 0.378 nm corresponds to the (110) planes of $\alpha\text{-MoO}_3$. [28, 29]

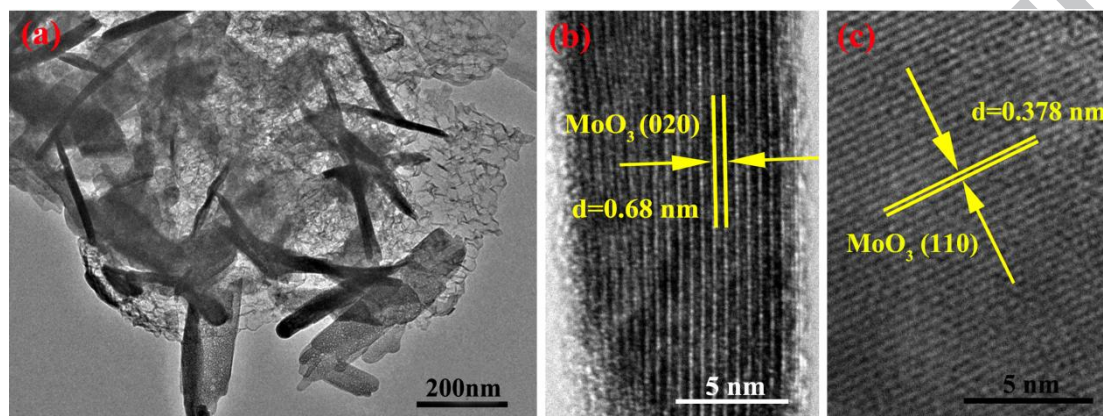


Figure 2. (a) TEM image of the MoO_3/CNFs , and (b) cross-view and (c) top-view HRTEM images taken from single MoO_3 nanoplates.

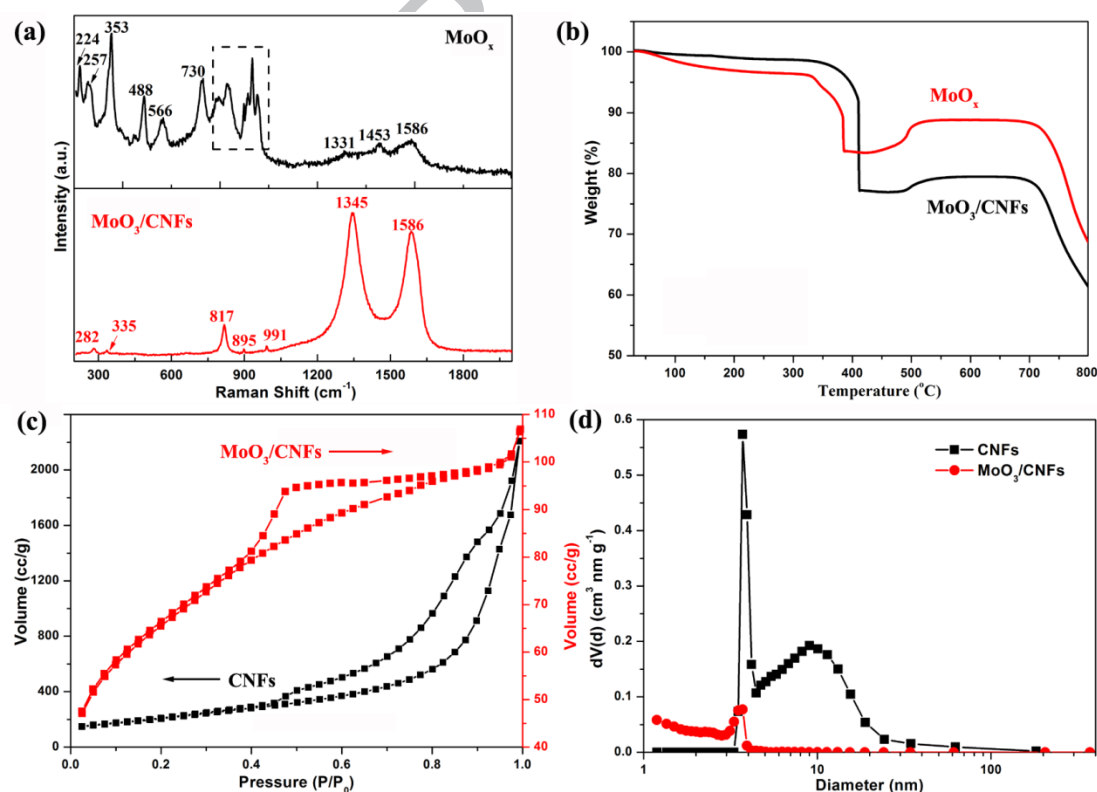


Figure 3. (a) Raman spectra and (b) TGA curves of the MoO_x and MoO_3/CNFs . (c) N_2 sorption isotherms and (d) the corresponding pore size distribution of the bare CNFs

and MoO₃/CNFs.

Figure 3a shows the Raman spectra of the MoO_x and MoO₃/CNFs. For MoO₃/CNFs, two prominent peaks at 1345 and 1586 cm⁻¹ correspond to D and G bands of CNFs, respectively. The peaks at 282 and 335 cm⁻¹ are ascribed to the bending modes of α -MoO₃ crystal, while the peaks at 817 and 991 cm⁻¹ are attributed to the intermediate bridging Mo-O-Mo bond and the vibration of the shortest Mo=O bonds.[30] In contrast, much more peaks are present in the MoO_x, and the peaks below 800 cm⁻¹ can all be related to MoO₂. [31] In addition to the two board peaks at 1331 and 1586 cm⁻¹, another peak appears at 1453 cm⁻¹, which can be indexed to the stretching vibration of carbon chain arising from the incomplete decomposition of the Mo precursor. The peaks in the range of 750-1000 cm⁻¹ indicate the intermediate oxidation state of MoO_x ($2 \leq x \leq 3$). [11, 31]

TGA analysis was used to determine the carbon content as well as the thermal stability of the MoO_x and MoO₃/CNFs. As shown in Figure 3c, it is obviously observed that both products show similar TGA profiles. For the MoO_x, apparent weight loss occurs at temperature above 100 °C and abruptly happens at 385 °C, indicating the incomplete decomposition of the Mo precursor after annealing in air at 300 °C. In contrast, MoO₃/CNFs undergoes sharp weight loss at about 410 °C which can be owing to the combustion of the CNFs, and the carbon content is determined to be about 22.7 wt.%. Besides, it should be noted that both products show weight increase at around 500 °C which may be due to further oxidation of the residual MoO_x. When further increasing the temperature to around 700 °C, there are abrupt weight loss in both sample, which can be attributed to the sublimation of MoO₃.

The specific surface areas as well as the pore structures of the CNFs and MoO₃/CNFs were further examined via N₂ adsorption-desorption isotherms. As shown in Figure 3c, the CNFs possess a high specific surface area of 751 m²/g, which greatly decreases to 225.7 m²/g for MoO₃/CNFs after the introduction of MoO₃. The pore size distribution of both products are compared in Figure 3d, which are derived from the desorption branch calculated according to the Barrett-Joyner-Halenda (BJH)

method. It's observed that the CNFs show a wide pore size distribution ranging from several to tens of nanometers. After introducing the MoO_3 nanoplates, the specific pore volume decreases greatly, indicating the uptake of the CNF pores by MoO_3 nanoplates as well as the residuals derived from the molybdenum 2-ethylhexanoate precursor.

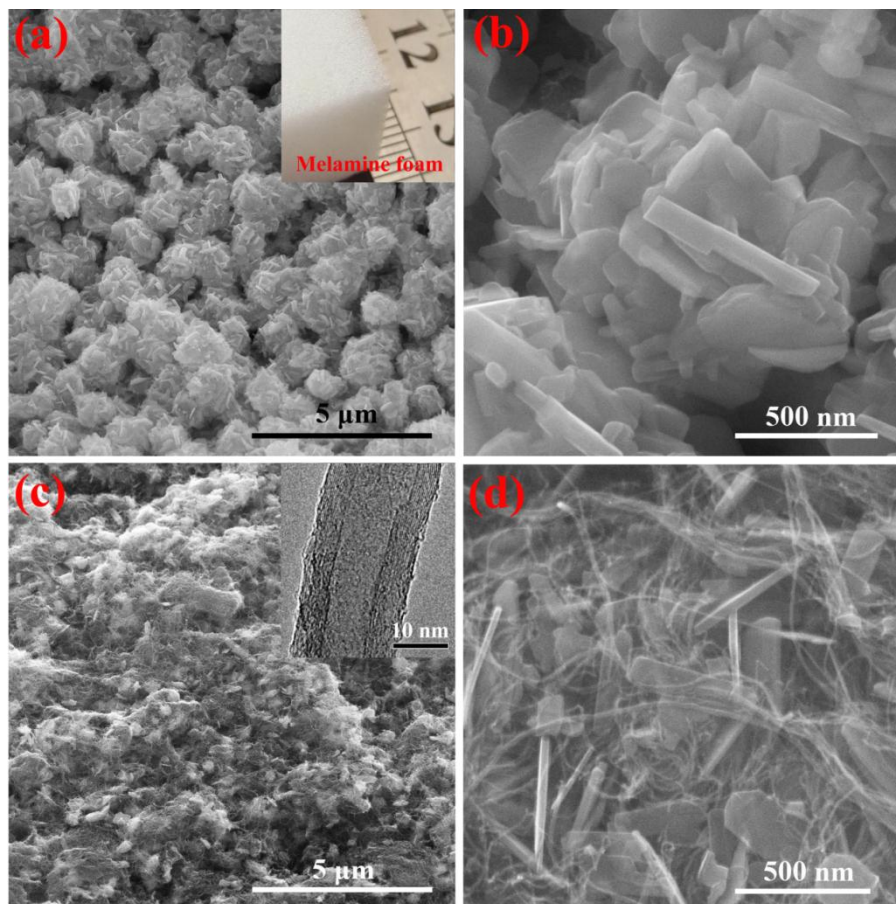


Figure 4. (a, b) SEM images of the aggregated MoO_3 nanoplates synthesized within the melamine foam (inset of a showing its digital photo). (c, d) SEM images of the MoO_3 nanoplates synthesized within CNTs (inset of c showing the TEM image of a single CNT).

More importantly, the current synthetic strategy can be generally applied for the hybridization of MoO_3 nanoplates with various other matrices. On the basis of the above results and discussion, we propose that the interconnected CNFs can host and dilute the molybdenum 2-ethylhexanoate precursor, allowing its adequate exposure into air, thus the decomposition of Mo precursor as well as the crystallization can be

efficiently proceeded. In order to verify this propose, we injected the molybdenum 2-ethylhexanoate into a commercial melamine foam and annealed at 500 °C in air, during which both underwent full decomposition. Figure 4a and b clearly reveal the generation of MoO₃ nanoplates, but which are thicker than that in MoO₃/CNFs and aggregated together into spheres owing to the large pore size of the melamine foam (inset of Figure 4a). Moreover, when replacing CNFs with CNTs²¹ (inset of Figure 4c) with other synthetic parameters kept constant, MoO₃ nanoplates are produced, which are intertwined by the CNTs (Figure 4c, d). Owing to the relative smaller specific surface area of the CNTs (330 m²/g), the thickness of the MoO₃ nanoplates in the MoO₃/CNTs is apparently larger than that in MoO₃/CNFs (Figure 1f vs. 4d). This further verifies the generality of the current synthetic strategy. Moreover, the relative contents of MoO₃ and CNFs (or other carbon-based materials) can be readily controlled through adjusting the introduction amount of molybdenum 2-ethylhexanoate and CNFs. Interestingly, the plate morphology of MoO₃ in the samples with different carbon content is well maintained, but the thickness and size are slightly different.

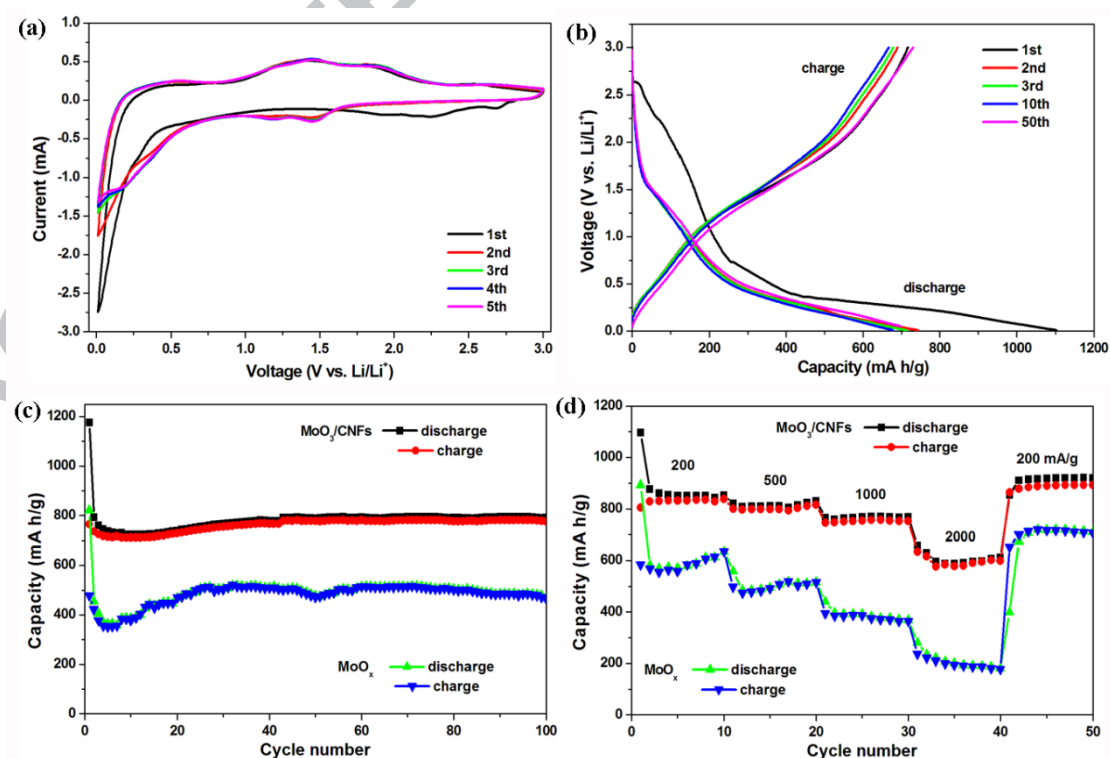


Figure 5. (a) CV curves and (b) discharge-charge profiles of the MoO₃/CNFs. (c)

Cycle performance at 500 mA/g and (d) rate performance at current densities ranging from 200 to 2000 mA/g for the MoO₃/CNFs and MoO_x electrodes.

The electrochemical properties of the MoO₃/CNFs as anode materials for LIBs were investigated in half-cells using lithium foil as reference and counter electrode. Figure 5a shows the CV curves of the MoO₃/CNFs electrode in the initial five cycles. In the first cathodic scan, two minor peaks at 2.68 and 2.25 V can be observed and then disappear in the following cycles, which correspond to the multistep intercalation processes of Li⁺ into the crystalline MoO₃ to form Li_xMoO₃, according to the reaction of $\text{MoO}_3 + x\text{Li}^+ + x\text{e}^- \rightarrow \text{Li}_x\text{MoO}_3$. [32, 33] This electrochemical reaction is irreversible, during which the crystalline MoO₃ converts into amorphous nonstoichiometric Li_xMoO₃. Notably, a strong cathodic peak appears at 0.02 V in the first cycle and then shifts to 0.2 V in the following cycles, which can be indexed to the reversible conversion reaction of $\text{Li}_x\text{MoO}_3 + (6-x)\text{Li}^+ + (6-x)\text{e}^- \leftrightarrow \text{Mo} + 3\text{Li}_2\text{O}$. [34] In the following cycles, two pairs of well-defined reversible redox located at 1.2/1.46 and 1.48/1.85 V are observed, which are commonly recognized as the amorphousization process of the MoO₃ active material. This result was attributed to a quasi-amorphous state of the cycled MoO₃ with decreased redox potentials. [35] In order to compare with pure MoO₃, the CV curves of a commercial MoO₃ with high purity and crystallinity were also measured, and the profiles are well consistent with the MoO₃/CNFs but with well-defined redox peaks (Figure S1). However, the CV curves of the MoO_x are not apparent owing to the poor crystallinity (as revealed by XRD in Figure 1a).

Figure 5b shows the galvanostatic discharge/charge profiles of the MoO₃/CNFs at the 1st, 2nd, 10th and 50th cycle in a voltage range of 0.01-3.0 V at 500 mA/g. The initial discharge/charge capacities are 1102/716 mA h/g with an initial Coulombic efficiency of 64.9%. In the following cycles, the discharge/charge capacities for the 2nd, 10th and 50th cycles are 743/689, 678/667 and 697/730 mA h/g, respectively, exhibiting much higher Coulombic efficiency of 92.7%, 98.4% and 104.7%. The gradually increased specific capacity and Coulombic efficiency are common in the

transition metal oxide electrodes, which can be due to the catalytic effect of the in situ generated transition metal grains on the decomposition of electrolyte and thus resultant formation of the gel-like film on the electrode surface.[36, 37]

Figure 5c compares the cycling performance of the MoO_3/CNFs and MoO_x in the voltage range of 0.01-3.0 V at 500 mA/g. Apparently, the MoO_3/CNFs anode exhibits much better cycling performance than that of the MoO_x anode, delivering a much higher reversible discharge capacity of about 791 mA h/g after 100 cycles, while the capacity of MoO_x only remains 468 mA h/g after 100 cycles, indicating that the introduction of CNFs not only affects the morphology of the MoO_3 but also greatly enhances the electrochemical performance. Figure 5d compares the rate performances of the MoO_3/CNFs and MoO_x electrodes at various current densities ranging from 100 to 2000 mA/g. The discharge capacities for MoO_3/CNFs electrode are 853, 830, 768 and 612 mA h/g each after 10 cycles at 200, 500, 1000 and 2000 mA/g, respectively. When recovering the current density to 200 mA/g, a discharge capacity of 919 mA h/g is maintained after another 10 cycles, indicating the high rate capability. In contrast, the capacities of the MoO_x electrode with no CNFs introduced are much lower than that of the MoO_3/CNFs counterpart (Figure 5d). The electrochemical properties of the MoO_3/CNTs were also examined and shown in Figure S2. The lithium storage performance of MoO_3/CNTs is also largely improved as compared with the MoO_x counterpart, but which is slightly inferior to that of MoO_3/CNFs , indicating the efficacy of CNFs in improving the electrochemical performance. Table S1 summarized the syntheses and lithium storage properties of the MoO_3 -based anode materials, and the MoO_3/CNFs displayed the well acceptable specific capacity.

Electrochemical impedance spectroscopy (EIS) was further performed to reveal the electrode charge transfer resistance and the kinetics of the electrochemical process. Figure 6 exhibits the Nyquist plots of the fresh MoO_3/CNFs and MoO_x electrodes, where the semicircle diameter represents the charge transfer resistance (R_{ct}). It's clearly observed that the fresh MoO_3/CNFs electrode exhibits a low R_{ct} of around 180 Ω , while the MoO_x electrode shows a much larger semicircle diameter (over 1000 Ω), indicating the introduction of CNFs greatly enhances the charge transfer rate. In

addition, the inclined line slope at the low frequency is relating to the lithium-diffusion process,[38] and the much steeper inclined line of the MoO_3/CNFs electrode indicates the faster lithium ion diffusion in the MoO_3 nanoplates / CNFs hybrid electrode. *Ex situ* SEM analysis was also performed to reveal the morphology evolution after cycling (Figure S3-4), which showed that the CNF morphology was well preserved, even though the MoO_3 nanoplates lost their morphology owing to the amorphization after repeated lithiation/delithiation. The CNFs not only function as conductive networks but also serve as buffering matrices, which finally contributed to the superior electrochemical performance

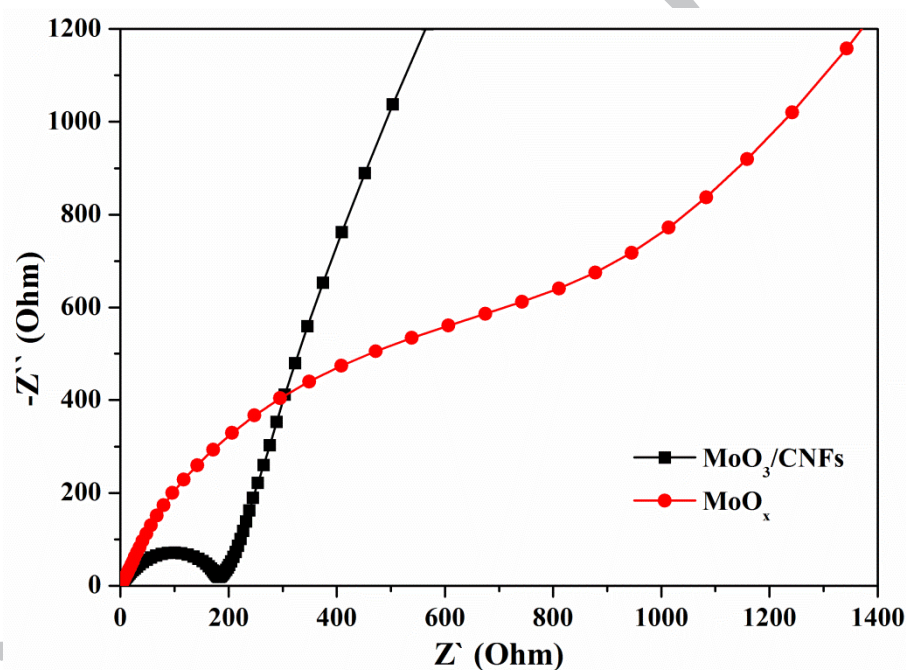


Figure 6. Nyquist plot of the fresh MoO_3/CNFs and MoO_x electrodes.

Conclusions

In summary, we have successfully developed an one-pot synthesis of MoO_3 nanoplates within foam-like carbon nanoflakes (CNFs) via pyrolysis of molybdenum 2-ethylhexanoate ($\text{C}_{48}\text{H}_{90}\text{MoO}_{12}$) at a low temperature of 300 °C under ambient atmosphere, which can be generally applied for fabrication of various MoO_3 /carbon-based nanocomposites. The current synthetic approach allows for the low-cost large-scale production and the easy control of the relative amount of the

MoO₃ and carbon contents by simply adjusting the introduction amount of the Mo precursor and carbon materials. Mixing C₄₈H₉₀MoO₁₂ with porous carbon materials (ex., CNFs) allows the sufficient pyrolysis of Mo precursor, facilitating the oriented crystallization of MoO₃ nanoplates. When used as anode material for LIBs, the optimized MoO₃/CNFs exhibited superior lithium storage performance, delivering a high discharge capacity of 791 mA h/g after 100 cycles at 500 mA/g and even ~600 mA h/g at a high rate of 2000 mA/g, which demonstrated great potential as high-performance electrodes for electrochemical energy-storage.

Acknowledgements.

This work was supported by the National Science Foundation of China (Grant No. 51402232) and the State Key Laboratory of Electrical Insulation and Power Equipment (No. EIPE17308). H.W. appreciates the support of the Tang Scholar Program from the Cyrus Tang Foundation.

References.

- [1] M.R. Palacín, Recent advances in rechargeable battery materials: a chemist's perspective, *Cheminform* 38(9) (2009) 2565-75.
- [2] H. Jiang, D.Y. Ren, H.F. Wang, Y.J. Hu, S.J. Guo, H.Y. Yuan, P.J. Hu, L. Zhang, C.Z. Li, 2D Monolayer MoS₂-Carbon Interoverlapped Superstructure: Engineering Ideal Atomic Interface for Lithium Ion Storage, *Adv. Mater.* 27(24) (2015) 3687-3695.
- [3] H. Wang, L. Xi, J. Tucek, C. Ma, G. Yang, M.K.H. Leung, R. Zboril, C. Niu, A.L. Rogach, Synthesis and Characterization of Tin Titanate Nanotubes: Precursors for Nanoparticulate Sn-Doped TiO₂ Anodes with Synergistically Improved Electrochemical Performance, *ChemElectroChem* 1(9) (2014) 1563-1569.
- [4] N.S. Choi, Z. Chen, S.A. Freunberger, X. Ji, Y.K. Sun, K. Amine, G. Yushin, L.F. Nazar, J. Cho, P.G. Bruce, Challenges facing lithium batteries and electrical double-layer capacitors, *Angewandte Chemie* 51(40) (2012) 9994.
- [5] S.H. Lee, Y.H. Kim, R. Deshpande, P.A. Parilla, E. Whitney, D.T. Gillaspie, K.M. Jones, A.H. Mahan, S.B. Zhang, A.C. Dillon, Reversible Lithium-Ion Insertion in Molybdenum Oxide Nanoparticles, *Advanced Materials* 20(19) (2008) 3627-3632.
- [6] D. Cao, H. Wang, B. Li, C. Li, S. Xie, A.L. Rogach, C. Niu, Hydrothermal Synthesis of SnO₂ Embedded MoO_{3-x} Nanocomposites and Their Synergistic Effects on Lithium Storage, *Electrochim. Acta* 216 (2016) 79-87.
- [7] Q. Xia, H.L. Zhao, Z.H. Du, Z.P. Zeng, C.H. Gao, Z.J. Zhang, X.F. Du, A. Kulka, K. Swierczek, Facile synthesis of MoO₃/carbon nanobelts as high-performance anode material for lithium ion

batteries, *Electrochim. Acta* 180 (2015) 947-956.

[8] X. Li, J.T. Xu, L. Mei, Z.J. Zhang, C.Y. Cui, H.K. Liu, J.M. Ma, S.X. Dou, Electrospinning of crystalline MoO₃@C nanofibers for high-rate lithium storage, *J Mater Chem A* 3(7) (2015) 3257-3260.

[9] H. Wang, A.L. Rogach, Hierarchical SnO₂ Nanostructures: Recent Advances in Design, Synthesis, and Applications, *Chem. Mater.* 26(1) (2014) 123-133.

[10] L.A. Riley, S.-H. Lee, L. Gedvilas, A.C. Dillon, Optimization of MoO₃ nanoparticles as negative-electrode material in high-energy lithium ion batteries, *Journal of Power Sources* 195(2) (2010) 588-592.

[11] P. Meduri, E. Clark, J.H. Kim, E. Dayalan, G.U. Sumanasekera, M.K. Sunkara, MoO₃-x Nanowire Arrays As Stable and High-Capacity Anodes for Lithium Ion Batteries, *Nano Letters* 12(4) (2012) 1784-1788.

[12] Z. Wang, S. Madhavi, X.W. Lou, Ultralong α -MoO₃ Nanobelts: Synthesis and Effect of Binder Choice on Their Lithium Storage Properties, *Journal of Physical Chemistry C* 116(23) (2012) 12508-12513.

[13] M.F. Hassan, Z.P. Guo, Z. Chen, H.K. Liu, Carbon-coated MoO₃ nanobelts as anode materials for lithium-ion batteries, *J. Power Sources* 195(8) (2010) 2372-2376.

[14] B. Ahmed, M. Shahid, D.H. Nagaraju, D.H. Anjum, M.N. Hedhili, H.N. Alshareef, Surface Passivation of MoO₃ Nanorods by Atomic Layer Deposition toward High Rate Durable Li Ion Battery Anodes, *ACS Appl. Mat. Interfaces* 7(24) (2015) 13154-13163.

[15] J.B. Zhou, N. Lin, L.B. Wang, K.L. Zhang, Y.C. Zhu, Y.T. Qian, Synthesis of hexagonal MoO₃ nanorods and a study of their electrochemical performance as anode materials for lithium-ion batteries, *J Mater Chem A* 3(14) (2015) 7463-7468.

[16] Y.N. Ko, S.B. Park, Y.C. Kang, Excellent Electrochemical Properties of Yolk-Shell MoO₃ Microspheres Formed by Combustion of Molybdenum Oxide-Carbon Composite Microspheres, *Chemistry-an Asian Journal* 9(4) (2014) 1011-1015.

[17] W.W. Xia, Q.B. Zhang, F. Xu, L.T. Sun, New Insights into Electrochemical Lithiation/Delithiation Mechanism of α -MoO₃ Nanobelt by in Situ Transmission Electron Microscopy, *Acs Applied Materials & Interfaces* 8(14) (2016) 9170-9177.

[18] Y.H. Li, H. Sun, X.P. Cheng, Y.F. Zhang, K.J. Zhao, In-situ TEM experiments and first -principles studies on the electrochemical and mechanical behaviors of α -MoO₃ in Li-ion batteries, *Nano Energy* 27 (2016) 95-102.

[19] T. Li, W. Zeng, Y. Zhang, S. Hussain, Nanobelt-assembled nest-like MoO₃ hierarchical structure: Hydrothermal synthesis and gas-sensing properties, *Materials Letters* 160 (2015) 476-479.

[20] J. Zhou, N. Lin, L. Wang, K. Zhang, Y. Zhu, Y. Qian, Synthesis of hexagonal MoO₃ nanorods and a study of their electrochemical performance as anode materials for lithium-ion batteries, *Journal of Materials Chemistry A* 3(14) (2015) 7463-7468.

[21] A. Gesheva K., T. Ivanova, A Low- Temperature Atmospheric Pressure CVD Process for Growing Thin Films of MoO₃ and MoO₃- WO₃ for Electrochromic Device Applications, *Chemical Vapor Deposition* 12(4) (2010) 231-238.

[22] G. Wang, Y. Ji, L. Zhang, Y. Zhu, P.-I. Gouma, M. Dudley, Synthesis of Molybdenum Oxide Nanoplatelets during Crystallization of the Precursor Gel from Its Hybrid Nanocomposites, *Chemistry of Materials* 19(5) (2007) 979-981.

[23] K. Dewangan, N.N. Sinha, P.K. Sharma, A.C. Pandey, N. Munichandraiah, N.S. Gajbhiye, Synthesis and characterization of single-crystalline α -MoO₃ nanofibers for enhanced Li-ion

intercalation applications, *Crystengcomm* 13(3) (2011) 927-933.

[24] M.B. Sreedhara, A.L. Santhosha, A.J. Bhattacharyya, C.N.R. Rao, Composite of few-layer MoO₃ nanosheets with graphene as a high performance anode for sodium-ion batteries, *Journal of Materials Chemistry A* 4(24) (2016) 9466-9471.

[25] H. Wang, J. Wang, D. Cao, H. Gu, B. Li, X. Lu, X. Han, A.L. Rogach, C. Niu, Honeycomb-like carbon nanoflakes as a host for SnO₂ nanoparticles allowing enhanced lithium storage performance, *Journal of Materials Chemistry A* (2017).

[26] Y. Li, X. Lu, H. Wang, C. Xie, G. Yang, C. Niu, Growth of Ultrafine SnO₂ Nanoparticles within Multiwall Carbon Nanotube Networks: Non-Solution Synthesis and Excellent Electrochemical Properties as Anodes for Lithium Ion Batteries, *Electrochimica Acta* 178 (2015) 778-785.

[27] H. Wang, J. Wang, D. Cao, H. Gu, B. Li, X. Lu, X. Han, A.L. Rogach, C. Niu, Honeycomb-like carbon nanoflakes as a host for SnO₂ nanoparticles allowing enhanced lithium storage performance, *J Mater Chem A* 5(15) (2017) 6817-6824.

[28] D. Chen, M. Liu, L. Yin, T. Li, Z. Yang, X. Li, B. Fan, H. Wang, R. Zhang, Z. Li, Single-crystalline MoO₃ nanoplates: topochemical synthesis and enhanced ethanol-sensing performance, *J Mater Chem* 21(25) (2011) 9332-9342.

[29] W. Tang, L. Liu, S. Tian, L. Li, Y. Yue, Y. Wu, K. Zhu, Aqueous supercapacitors of high energy density based on MoO₃ nanoplates as anode material, *Chemical Communications* 47(36) (2011) 10058-60.

[30] J. Ni, G. Wang, J. Yang, D. Gao, J. Chen, L. Gao, Y. Li, Carbon nanotube-wired and oxygen-deficient MoO₃ nanobelts with enhanced lithium-storage capability, *Journal of Power Sources* 247 (2014) 90-94.

[31] L. Kumari, Y.R. Ma, C.C. Tsai, Y.W. Lin, S.Y. Wu, K.W. Cheng, Y. Liou, X-ray diffraction and Raman scattering studies on large-area array and nanobranched structure of 1D MoO₂ nanorods, *Nanotechnology* 18(11) (2007) 115717.

[32] Z. Wang, S. Madhavi, X.W. Lou, Ultralong alpha-MoO₃ Nanobelts: Synthesis and Effect of Binder Choice on Their Lithium Storage Properties, *Journal of Physical Chemistry C* 116(23) (2012) 12508-12513.

[33] Y. Sun, J. Wang, B. Zhao, R. Cai, R. Ran, Z. Shao, Binder-free alpha-MoO₃ nanobelt electrode for lithium-ion batteries utilizing van der Waals forces for film formation and connection with current collector, *Journal of Materials Chemistry A* 1(15) (2013) 4736-4746.

[34] X. Zhang, X. Song, S. Gao, Y. Xu, X. Cheng, H. Zhao, L. Huo, Facile synthesis of yolk-shell MoO₂ microspheres with excellent electrochemical performance as a Li-ion battery anode, *Journal of Materials Chemistry A* 1(23) (2013) 6858-6864.

[35] F. Ma, A. Yuan, J. Xu, P. Hu, Porous α -MoO₃/MWCNT Nanocomposite Synthesized via a Surfactant-Assisted Solvothermal Route as a Lithium-Ion-Battery High-Capacity Anode Material with Excellent Rate Capability and Cyclability, *ACS Appl. Mat. Interfaces* 7(28) (2015) 15531-15541.

[36] S. Laruelle, S. Grugeon, P. Poizot, M. Dollé, L. Dupont, J.M. Tarascon, On the Origin of the Extra Electrochemical Capacity Displayed by MO/Li Cells at Low Potential, *Journal of the Electrochemical Society* 149(5) (2002) A627-A634.

[37] D. Cao, H. Wang, B. Li, C. Li, S. Xie, A.L. Rogach, C. Niu, Hydrothermal Synthesis of SnO₂ Embedded MoO_{3-x} Nanocomposites and Their Synergistic Effects on Lithium Storage, *Electrochimica Acta* 216 (2016) 79-87.

[38] J. Guo, A. Sun, X. Chen, C. Wang, A. Manivannan, Cyclability study of silicon-carbon composite

anodes for lithium-ion batteries using electrochemical impedance spectroscopy, *Electrochimica Acta* 56(11) (2011) 3981-3987.

ACCEPTED MANUSCRIPT

Graphical abstract

